JACS
JOURNAL OF THE AMERICAN CHEMICAL SOCIETY
Communication
pubs.acs.org/JACS

The Cu-CHA deNO$_x$ Catalyst in Action: Temperature-Dependent NH$_3$-Assisted Selective Catalytic Reduction Monitored by Operando XAS and XES

Kirill A. Lomachenko,[†,‡] Elisa Borfecchia,[*,†] Chiara Negri,[†] Gloria Berlier,[†] Carlo Lamberti,[†,‡] Pablo Beato,[§] Hanne Falsig,[§] and Silvia Bordiga[†]

[†]Department of Chemistry, NIS Centre and INSTM Reference Center, University of Turin, via P. Giuria 7, 10125 Turin, Italy
[‡]IRC "Smart Materials", Southern Federal University, Zorge Street 5, 344090 Rostov-on-Don, Russia
[§]Haldor Topsøe A/S, Haldor Topsøes Allé 1, 2800 Kgs. Lyngby, Denmark

Supporting Information

ABSTRACT: The small-pore Cu-CHA zeolite is today the object of intensive research efforts to rationalize its outstanding performance in the NH$_3$-assisted selective catalytic reduction (SCR) of harmful nitrogen oxides and to unveil the SCR mechanism. Herein we exploit operando X-ray spectroscopies to monitor the Cu-CHA catalyst in action during NH$_3$-SCR in the 150−400 °C range, targeting Cu oxidation state, mobility, and preferential N or O ligation as a function of reaction temperature. By combining operando XANES, EXAFS, and vtc-XES, we unambiguously identify two distinct regimes for the atomic-scale behavior of Cu active-sites. Low-temperature SCR, up to ∼200 °C, is characterized by balanced populations of Cu(I)/Cu(II) sites and dominated by mobile NH$_3$-solvated Cu-species. From 250 °C upward, in correspondence to the steep increase in catalytic activity, the largely dominant Cu-species are framework-coordinated Cu(II) sites, likely representing the active sites for high-temperature SCR.

Recent years have seen a renaissance for metal-exchanged zeolites. These systems are attracting growing interest as versatile platforms for novel chemistry at the boundary between homogeneous and heterogeneous catalysis. Copper, with its rich redox chemistry and exquisite coordinative flexibility, as we see in many Cu-enzymes,[1,2] is the ideal candidate for single-site catalysis empowered by host−guest interactions inside the zeolite cages. In particular, the small-pore Cu-CHA zeolite is today the object of intensive research efforts to rationalize its outstanding performance in the NH$_3$-assisted selective catalytic reduction (SCR) of harmful nitrogen oxides.[3−7] Cu-CHA is currently commercialized due to its enhanced activity, selectivity, and hydrothermal stability[8] with respect to other zeolite-based catalysts. Despite the recent advances in the understanding of the SCR mechanism on Cu-CHA,[6,9−15] several questions still need to be addressed to design deNO$_x$ catalysts able to keep pace with the increasingly stricter regulations worldwide.

The powerful experimental and theoretical methods matured in the past decade are enabling an unprecedented molecular-level understanding of the structure−composition−activity relationship in Cu-zeolites. Very recently, Paolucci et al.[15] have synergized experiment and theory to correlate the compositional parameters in Cu-CHA and the types/numbers of Cu-sites formed after dehydration and in SCR-relevant conditions. The authors demonstrated that during dehydration Cu(II) ions first populate 2Al sites in the six-membered rings (6r) of the CHA framework (Z_2-Cu(II), where Z_2 denotes two neighboring charge-balancing framework Al sites), identified as the most energetically favored exchange sites for "naked" Cu(II) ions.[16,17] Once the less reducible[11,15,18,19] Z_2-Cu(II) sites are saturated, Cu cations are stabilized in proximity of isolated 1Al sites as redox-active Z-[Cu(II)OH$^-$] complexes (where Z denotes an isolated framework Al site), representing the dominant coordination environment at high Cu-loading.[19,20] Importantly, the chemical and spectroscopic distinction between these two types of Cu-sites is less pronounced when the catalyst is exposed to the SCR feed or partial mixtures of SCR reactants. Consistently with previous reports,[21,22] operando XANES during SCR at 200 °C revealed the presence of a ∼50/50% Cu(I)/Cu(II) mixture. Paolucci et al.[15] associated the Cu(I) and Cu(II) components to the most stable species evidenced by DFT: Z[Cu(I) $(NH_3)_2$] (also observed after exposure to the NO + NH$_3$ mixture at 200 °C, as was reported before[12,13,23]) and Z[Cu(II)OH$(NH_3)_3$] on 1Al sites; Z_2[Cu(II) $(NH_3)_4$] and Z[NH_4^+]/Z[Cu(I) $(NH_3)_2$] on 2Al sites. On this basis, NH$_3$-solvated Cu-complexes, scarcely interacting with CHA framework and poorly influenced by Al distribution, are proposed as the SCR active sites at 200 °C. On the other hand, the authors suggest that NH$_3$ desolvation at higher temperature is expected to influence the SCR rates, especially in the oxidation half-cycle. Since no evidence on this key aspect has been reported so far, a temperature-dependent investigation of the Cu-CHA catalyst in action during NH$_3$ SCR becomes crucial to pinpoint alternative reaction pathways and Cu active species as a function of the operation temperature. To bridge this gap, we monitored Cu-CHA during NH$_3$ SCR in the 150−400 °C range by operando XAS and XES,[5,7,24−31] tracking (i) oxidation state, (ii) mobility, and (iii) preferential N or O ligation for Cu sites as a function of

Received: July 1, 2016
Published: August 17, 2016

DOI: 10.1021/jacs.6b06809
J. Am. Chem. Soc. 2016, 138, 12025−12028

reaction temperature. From these experiments, it clearly emerges that temperature strongly influences Cu-speciation during SCR, with profound implications on the elucidation of SCR active sites and mechanism. We performed operando XAS/XES during standard SCR (500 ppm of NO, 500 ppm of NH_3, 5% H_2O, 10% O_2/He, flow rate = 300 mL/min) using a well-established gas flow setup on a Cu-CHA catalyst with composition (Si/Al = 15, Cu/Al = 0.48) equivalent to the one investigated in our previous studies[13,19,23] and selected by Paolucci et al.[15] as the reference for 1Al site-containing Cu-CHA. In such compositional ranges, 2Al sites are known to occur only as minority Cu-species,[15,18,19] and are hence not considered in the data analysis (see SI, Section 3). Additional details on sample synthesis and experimental setup are reported in SI, Section 1). A mass spectrometer downstream the reactor cell allowed us to qualitatively verify that the catalyst was active for SCR reaction during XAS/XES measurements, whereas temperature-dependent SCR rates were obtained in dedicated laboratory tests on the same catalyst batch (see also SI, Section 2).

Figure 1 shows the temperature-dependent modifications in the XANES of Cu-CHA during SCR. To guide data

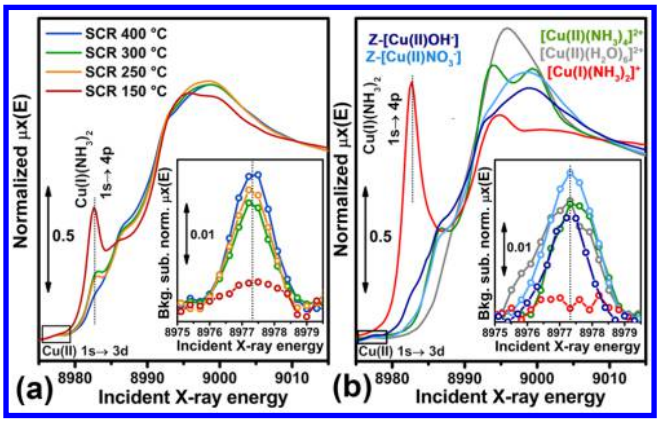

Figure 1. (a) Operando XANES collected during SCR at temperatures of 150, 250, 300, 400 °C. (b) XANES spectra of selected reference Cu-species employed to interpret operando data reported in part (a). Corresponding axes scale in parts (a) and (b) is the same. Insets report a magnification of the background-subtracted Cu(II) 1s → 3d pre-edge peaks (black boxes in the main panels).

interpretation, operando XANES (Figure 1a) are compared to the ones obtained for a series or references (Figure 1b), selected considering the principal spectral features emerging during SCR. Reference XANES spectra were separately measured for Cu(I) and Cu(II) aqua/amino complexes in solution (m-Cu(I) and m-Cu(II), m = "mobile") and framework-interacting Cu(II) species in Cu-CHA (Z-Cu(II)), namely three-coordinated Z-[Cu(II)OH^-] and four-coordinated Z-[Cu(II)NO_3^-] (see SI, Section 3.1). To estimate temperature-dependent Cu-speciation during SCR, we applied linear combination fit (LCF) analysis using the reference spectra in Figure 1b (see SI, Section 3.2). The operando SCR XANES spectrum at 150 °C is in excellent agreement with the observations reported by Paolucci et al. and others[15,21,22] during standard SCR at 200 °C. Hence, our experimental conditions guarantee a reliable comparison with previous studies. The pre-edge peak at ∼8977.3 eV, mostly arising from Cu(II) 1s → 3d transition,[32,33] is significantly lower than in Cu(II) references. The characteristic edge-rising peak at ∼8982.5 eV, deriving from 1s → 4p transition in the linear Cu(I) $(NH_3)_2$ complex,[32,34] is well evident. LCF indicates a ∼46% contribution from m-Cu(I), in the form of [Cu(I)$(NH_3)_2]^+$, whereas the remaining XANES signal is fitted with an almost equal fraction of Z-Cu(II) (∼26%) and m-Cu(II) (∼25%) species. In other words, "mobile" Cu(II) and Cu(I) sites solvated by ammonia are the main sites, in agreement with Paolucci et al.,[15] with a small fraction of Cu(II) sites interacting with the framework. Crucially, an abrupt modification in the operando XANES is observed from 250 °C and upward. The contribution of m-Cu(I) reduces to ∼15%, and the spectral shape evolves toward the one characteristic of Z-Cu(II): an edge-rising shoulder at ∼8986.6 eV and a broad white line peak centered at 8997.7 eV, typically increasing in intensity for four-coordinated Z-Cu(II) sites with respect to three-coordinated ones (e.g., compare the Z-[Cu(II)OH^-] and Z-[Cu(II)NO_3^-] references in Figure 1b).[13,19] Z-Cu(II) species collectively account for ∼74% of Cu sites (the remaining 11% attributed to minor contributions from m-Cu(II) complexes). The remarkable intensity increase of the Cu(II) 1s → 3d pre-edge peak clearly indicates a largely dominant 2+ oxidation state, in agreement with LCF results. A further increase in the operation temperature induces more subtle but still appreciable modifications. At 300 °C, the relative contributions from mobile and framework-interacting species remain almost unchanged, whereas the slight intensity decrease observed in the white line region is compatible with the partial conversion of four-coordinated Z-Cu(II) sites into three-coordinated ones. This trend is maintained at 400 °C. Here LCF evidences negligible contributions from m-Cu(I) and m-Cu(II) species and largely dominant Z-Cu(II) sites preferentially occurring as three-coordinated sites.

Operando EXAFS and XES allowed us to independently validate the XANES results described above, targeting the mobility level and the preferential O- or N-ligation of the Cu active sites, respectively. It is now established[13,15,19,21] that the well-defined maximum at ∼2.3 Å in the phase-uncorrected modulus of FT-EXAFS spectrum of dehydrated Cu-CHA derives from single-scattering paths involving Al/Si atoms of the CHA framework. Although the variable-temperature data collection and the presence of multiple Cu-species prevent a quantitative fitting of operando EXAFS, the second-shell peak at 2.3 Å can be exploited as a fingerprint for framework-coordinated Cu-sites. As shown in Figure 2a, this EXAFS feature is always present during SCR in the (250−400) °C range, with stable intensity and shape comparable with what observed for Z-Cu(II) references (Figure 2b). In the same temperature interval, we notice slight fluctuations in the first-shell intensity of the operando EXAFS spectra, suggesting an increase in the average first-shell coordination number as temperature decreases. Interestingly, in the high-R range, the FT-EXAFS at 250 °C seems more similar to the Z-[Cu(II)NO_3^-] reference, since a well-defined maximum at ∼3.2 Å was connected to a multiple-scattering feature peculiar of bidentate Z-[Cu(II)NO_3^-] moieties[13] (see SI, Section 4). The EXAFS signature of the Cu-CHA catalyst drastically changes when SCR is run at 150 °C. The second-shell maximum is strongly perturbed and partially evolves toward the unstructured shape characteristic of m-Cu(I)/(II) species. The first-shell intensity decreases despite the drop of thermal contribution to the Debye−Waller factors, consistently with an increase of the fraction of two-coordinated species with N/O ligands, which are hardly distinguishable by XAS.

DOI: 10.1021/jacs.6b06809
J. Am. Chem. Soc. 2016, 138, 12025−12028

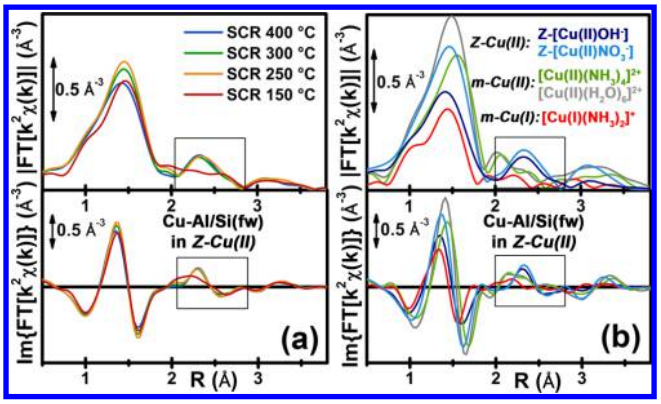

Figure 2. (a) Operando phase-uncorrected FT-EXAFS spectra (moduli and imaginary parts of FT in top and bottom panel, respectively) during SCR at 150, 250, 300, 400 °C. (b) Phase-uncorrected FT-EXAFS spectra of selected Cu-references employed to interpret operando data reported in part (a). In both part (a) and (b) all the FT-EXAFS spectra are calculated transforming k^2-weighted $\chi(k)$ spectra in the range 2.5−12.4 Å^{-1} (see SI, Section 4). Corresponding axes scale in parts (a) and (b) is the same.

As already shown in in situ/operando studies on Cu-CHA,[14,23,35] such an ambiguity regarding the type of ligands can be resolved by valence-to-core (vtc) XES, monitoring the energy position of the weak Kβ'' satellite.[28,36] Moreover, the overall K$\beta_{2,5}$ line shape is highly sensitive to local coordination geometry and symmetry and represents a valid support to qualitatively cross-check Cu-speciation from XANES.

Figure 3 shows operando SCR XES spectra for key temperature points (Figure 3a), together with representative

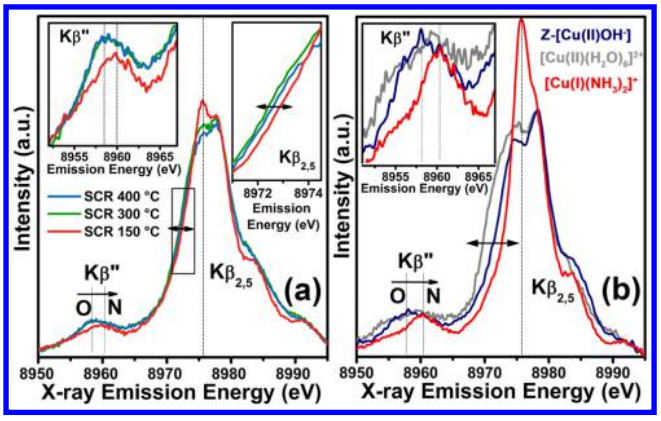

Figure 3. (a) Background-subtracted operando XES spectra collected during SCR at temperatures of 150, 300, 400 °C. (b) Background-subtracted XES spectra of selected Cu references states formed inside the pores of Cu-CHA, representative of Z-Cu(II), m-Cu(II) and m-Cu(I) species. The insets report magnifications of the Kβ'' satellites and, for part (a) only, of the left side of the K$\beta_{2,5}$ line, highlighted by the black boxes in the main panels.

reference XES data for Z-Cu(II), m-Cu(II), and m-Cu(I) species formed inside the pores of Cu-CHA (Figure 3b), see also SI Sections 1.5 and 3.1. As for operando XANES and EXAFS data sets, two distinct regimes can be individuated. In the high-temperature range, at 400 and 300 °C, the K$\beta_{2,5}$ line shape characteristic of Z-Cu(II) species is observed, and the energy position of the Kβ'' peak reveals largely dominant O ligation. Conversely, at 150 °C the K$\beta_{2,5}$ line shape clearly evolves toward the one observed for Cu(I) $(NH_3)_2$, characterized by a narrow and intense peak at ∼8976 eV. In parallel, the Kβ'' satellite significantly shifts to higher energy, unambiguously indicating a substantial increase in the fraction of N-coordinated Cu-species in the catalyst. The Kβ'' energy position observed in these conditions is intermediate between the ones observed for pure O and N ligation, in agreement with XANEX LCF analysis (60% of NH_3-solvated Cu-species, largely present as $[Cu(I)(NH_3)_2]^{2+}$. In addition, the broad feature on the low-energy side of the K$\beta_{2,5}$ peak, typical of hydrated Cu(II) ions (see Figure 3b, gray curve), is never observed in the operando XES series, supporting a very minor H_2O coordination in the whole probed temperature range. Consistently with LCF XANES and with many FTIR evidence reported before,[23,37] in the low-temperature SCR range, Cu-ions are almost exclusively solvated and mobilized by NH_3.

In conclusion, operando XAS/XES during SCR unambiguously point out that two distinct regimes exist for the atomic-scale behavior of Cu-sites in the investigated Cu-CHA catalyst, emerging at different temperature ranges. As depicted in Figure 4, low-temperature SCR, up to ∼200 °C, is characterized by balanced populations of Cu(I)/Cu(II) sites and dominated by mobile NH_3-solvated Cu-species.

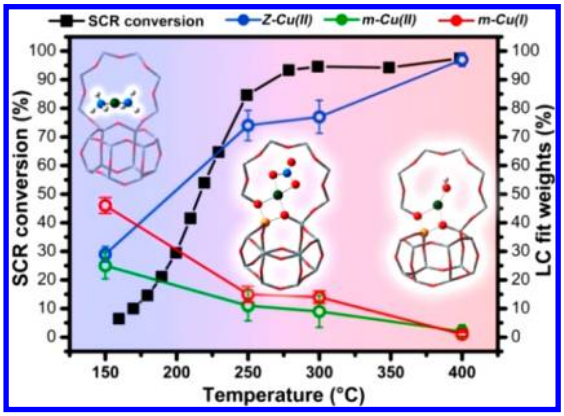

Figure 4. Comparison between temperature-dependent NH_3 SCR conversion rate and Cu-speciation in Cu-CHA. Structural snapshots of the dominant (highest relative abundance over the total number of Cu sites) model Cu-species evidenced by LCF analysis of operando XANES for each probed temperature are also reported, including Z-$[Cu(II)OH^-]$ and Z-$[Cu(II)NO_3^-]$ in the high-temperature range and mobile Cu(I) $(NH_3)_2$ complexes in the low-temperature range (atoms color code: Cu: green, O: red, Al: yellow, Si: gray, N: blue, H: white).

Noteworthy, operando FT-EXAFS do not show any signal ascribable to Cu-Cu scattering paths. Hence, at our experimental conditions, most of Cu occurs as monomeric species, although a minor high-R contribution from neighboring Cu-sites, proposed to favor NO activation by O_2[13b] cannot be excluded. We fully agree with Paolucci et al.[15] in assigning the Cu(I) component to Z$[Cu(I)(NH_3)_2]$ species. As for the Cu(II) component, assigned by Paolucci et al. to Z-$[Cu(II)OH(NH_3)_3]$ species, results of our LCF analysis demonstrate that it can be as well ascribed to a complex mixture of residual O-bonded Z-Cu(II) sites and m-Cu(II) complexes (mostly with NH_3 ligands). In the 250−400 °C range, a completely different scenario is revealed: Cu is largely present as framework-coordinated Z-Cu(II) species, accounting for ∼70% to more than 90% of total Cu sites. Here, temperature-dependent dynamics seems to mostly involve Cu interaction with O-bonding extra-framework groups and

DOI: 10.1021/jacs.6b06809
J. Am. Chem. Soc. 2016, 138, 12025−12028

reactants from the gas phase (e.g., hydroxyls and bidentate nitrates/nitrites), while coordination to framework is substantially unperturbed. Very interestingly, the transition between these two regimes corresponds to the steep rise in the temperature-dependent SCR conversion rate, determined in an independent catalytic test (see SI, Section 1.2) and reported in Figure 4 for comparison. These novel findings evidence a profound influence of the operation conditions on Cu-speciation during NH_3 SCR, which should be considered to fully unleash the potential of Cu-zeolite based deNO_x catalysts.

■ ASSOCIATED CONTENT

Supporting Information

The Supporting Information is available free of charge on the ACS Publications website at DOI: 10.1021/jacs.6b06809.

Experimental and data analysis details (PDF)

■ AUTHOR INFORMATION

Corresponding Author

*elisa.borfecchia@unito.it

Notes

The authors declare no competing financial interest.

■ ACKNOWLEDGMENTS

C.L. and K.A.L. acknowledge the Mega-grant of the Russian Federation Government no. 14.Y26.31.0001. K.A.L acknowledges the scholarship of the President of Russia for Ph.D. students and young scientists no. СП-2796.2016.1. E.B. acknowledges Innovation Fund Denmark (Industrial postdoc no. 5190-00018B). We thank G. Agostini, O. Mathon, S. Gatla, P. Glatzel, E. Gallo, K. Kvashnina for their help during the ESRF beamtime on BM23 and ID26 and F. Giordanino, C. Tyrsted, T. V. W. Janssens, P. N. R. Vennestrøm, and A. Puig-Molina for support during data collection and insightful discussions.

■ REFERENCES

(1) Solomon, E. I.; Heppner, D. E.; Johnston, E. M.; Ginsbach, J. W.; Cirera, J.; Qayyum, M.; Kieber-Emmons, M. T.; Kjaergaard, C. H.; Hadt, R. G.; Tian, L. *Chem. Rev.* **2014**, *114*, 3659.

(2) Lee, J. Y.; Karlin, K. D. *Curr. Opin. Chem. Biol.* **2015**, *25*, 184.

(3) Brandenberger, S.; Krocher, O.; Tissler, A.; Althoff, R. *Catal. Rev.: Sci. Eng.* **2008**, *50*, 492.

(4) Granger, P.; Parvulescu, V. I. *Chem. Rev.* **2011**, *111*, 3155.

(5) Deka, U.; Lezcano-Gonzalez, I.; Weckhuysen, B. M.; Beale, A. M. *ACS Catal.* **2013**, *3*, 413.

(6) Gao, F.; Kwak, J.; Szanyi, J.; Peden, C. F. *Top. Catal.* **2013**, *56*, 1441.

(7) Beale, A. M.; Gao, F.; Lezcano-Gonzalez, I.; Peden, C. H. F.; Szanyi, J. *Chem. Soc. Rev.* **2015**, *44*, 7371.

(8) Kwak, J. H.; Tran, D.; Burton, S. D.; Szanyi, J.; Lee, J. H.; Peden, C. H. F. *J. Catal.* **2012**, *287*, 203.

(9) Kwak, J. H.; Lee, J. H.; Burton, S. D.; Lipton, A. S.; Peden, C. H. F.; Szanyi, J. *Angew. Chem., Int. Ed.* **2013**, *52*, 9985.

(10) Gao, F.; Walter, E. D.; Kollar, M.; Wang, Y.; Szanyi, J.; Peden, C. H. F. *J. Catal.* **2014**, *319*, 1.

(11) Gao, F.; Washton, N. M.; Wang, Y. L.; Kollar, M.; Szanyi, J.; Peden, C. H. F. *J. Catal.* **2015**, *331*, 25.

(12) Paolucci, C.; Verma, A. A.; Bates, S. A.; Kispersky, V. F.; Miller, J. T.; Gounder, R.; Delgass, W. N.; Ribeiro, F. H.; Schneider, W. F. *Angew. Chem., Int. Ed.* **2014**, *53*, 11828.

(13) (a) Janssens, T. V. W.; Falsig, H.; Lundegaard, L. F.; Vennestrøm, P. N. R.; Rasmussen, S. B.; Moses, P. G.; Giordanino, F.; Borfecchia, E.; Lomachenko, K. A.; Lamberti, C.; Bordiga, S.; Godiksen, A.; Mossin, S.; Beato, P. *ACS Catal.* **2015**, *5*, 2832. (b) Falsig, H.; Vennestrøm, P. N. R.; Moses, P. G.; Janssens; Ton, V. W. *Top. Catal.* **2016**, *59*, 861.

(14) Günter, T.; Carvalho, H. W. P.; Doronkin, D. E.; Sheppard, T.; Glatzel, P.; Atkins, A. J.; Rudolph, J.; Jacob, C. R.; Casapu, M.; Grunwaldt, J. D. *Chem. Commun.* **2015**, *51*, 9227.

(15) Paolucci, C.; Parekh, A. A.; Khurana, I.; Di Iorio, J. R.; Li, H.; Albarracin Caballero, J. D.; Shih, A. J.; Anggara, T.; Delgass, W. N.; Miller, J. T.; Ribeiro, F. H.; Gounder, R.; Schneider, W. F. *J. Am. Chem. Soc.* **2016**, *138*, 6028.

(16) Korhonen, S. T.; Fickel, D. W.; Lobo, R. F.; Weckhuysen, B. M.; Beale, A. M. *Chem. Commun.* **2011**, *47*, 800.

(17) Deka, U.; Juhin, A.; Eilertsen, E. A.; Emerich, H.; Green, M. A.; Korhonen, S. T.; Weckhuysen, B. M.; Beale, A. M. *J. Phys. Chem. C* **2012**, *116*, 4809.

(18) Godiksen, A.; Stappen, F. N.; Vennestrom, P. N. R.; Giordanino, F.; Rasmussen, S. B.; Lundegaard, L. F.; Mossin, S. *J. Phys. Chem. C* **2014**, *118*, 23126.

(19) Borfecchia, E.; Lomachenko, K. A.; Giordanino, F.; Falsig, H.; Beato, P.; Soldatov, A. V.; Bordiga, S.; Lamberti, C. *Chem. Sci.* **2015**, *6*, 548.

(20) Giordanino, F.; Vennestrom, P. N. R.; Lundegaard, L. F.; Stappen, F. N.; Mossin, S. L.; Beato, P.; Bordiga, S.; Lamberti, C. *Dalton Trans.* **2013**, *42*, 12741.

(21) McEwen, J. S.; Anggara, T.; Schneider, W. F.; Kispersky, V. F.; Miller, J. T.; Delgass, W. N.; Ribeiro, F. H. *Catal. Today* **2012**, *184*, 129.

(22) Bates, S. A.; Verma, A. A.; Paolucci, C.; Parekh, A. A.; Anggara, T.; Yezerets, A.; Schneider, W. F.; Miller, J. T.; Delgass, W. N.; Ribeiro, F. H. *J. Catal.* **2014**, *312*, 87.

(23) Giordanino, F.; Borfecchia, E.; Lomachenko, K. A.; Lazzarini, A.; Agostini, G.; Gallo, E.; Soldatov, A. V.; Beato, P.; Bordiga, S.; Lamberti, C. *J. Phys. Chem. Lett.* **2014**, *5*, 1552.

(24) Lomachenko, K. A.; Borfecchia, E.; Bordiga, S.; Soldatov, A. V.; Beato, P.; Lamberti, C. *J. Phys.: Conf. Ser.* **2016**, *712*, 012041.

(25) Bordiga, S.; Groppo, E.; Agostini, G.; van Bokhoven, J. A.; Lamberti, C. *Chem. Rev.* **2013**, *113*, 1736.

(26) Mino, L.; Agostini, G.; Borfecchia, E.; Gianolio, D.; Piovano, A.; Gallo, E.; Lamberti, C. *J. Phys. D: Appl. Phys.* **2013**, *46*, 423001.

(27) Garino, C.; Borfecchia, E.; Gobetto, R.; Salassa, L.; van Bokhoven, J. A.; Lamberti, C. *Coord. Chem. Rev.* **2014**, *277*−*278*, 130.

(28) Glatzel, P.; Bergmann, U. *Coord. Chem. Rev.* **2005**, *249*, 65.

(29) Smolentsev, G.; Soldatov, A. V.; Messinger, J.; Merz, K.; Weyhermuller, T.; Bergmann, U.; Pushkar, Y.; Yano, J.; Yachandra, V. K.; Glatzel, P. *J. Am. Chem. Soc.* **2009**, *131*, 13161.

(30) Singh, J.; Lamberti, C.; van Bokhoven, J. A. *Chem. Soc. Rev.* **2010**, *39*, 4754.

(31) *X-Ray Absorption and X-ray Emission Spectroscopy: Theory and Application*; van Bokhoven, J. A., Lamberti, C., Eds.; John Wiley & Sons: Chichester, U.K., 2016.

(32) Kau, L. S.; Spirasolomon, D. J.; Pennerhahn, J. E.; Hodgson, K. O.; Solomon, E. I. *J. Am. Chem. Soc.* **1987**, *109*, 6433.

(33) Sano, M.; Komorita, S.; Yamatera, H. *Inorg. Chem.* **1992**, *31*, 459.

(34) (a) Lamble, G.; Moen, A.; Nicholson, D. G. *J. Chem. Soc., Faraday Trans.* **1994**, *90*, 2211. (b) Mathisen, K.; Stockenhuber, M.; Nicholson, D. G. *Phys. Chem. Chem. Phys.* **2009**, *11*, 5476.

(35) Günter, T.; Doronkin, D. E.; Boubnov, A.; Carvalho, H. W. P.; Casapu, M.; Grunwaldt, J.-D. *Top. Catal.* **2016**, *59*, 866.

(36) Vegelius, J. R.; Kvashnina, K. O.; Klintenberg, M.; Soroka, I. L.; Butorin, S. M. *J. Anal. At. Spectrom.* **2012**, *27*, 1882.

(37) Lezcano-Gonzalez, I.; Deka, U.; Arstad, B.; Van Yperen-De Deyne, A.; Hemelsoet, K.; Waroquier, M.; Van Speybroeck, V.; Weckhuysen, B. M.; Beale, A. M. *Phys. Chem. Chem. Phys.* **2014**, *16*, 1639.

DOI: 10.1021/jacs.6b06809
J. Am. Chem. Soc. 2016, 138, 12025−12028